Received: 4 January 2018 | Accepted: 18 May 2018

DOI: 10.1111/ijag.12356

INTERNATIONAL JOURNAL OF
Applied Glass
SCIENCE

ORIGINAL ARTICLE

A Raman investigation of the structural evolution of supercooled liquid barium disilicate during crystallization

Benjamin J. A. Moulton[1,2] | **Alisson Mendes Rodrigues**[2] | **Paulo Sergio Pizani**[1,2] | **David Vieira Sampaio**[1,2] | **Edgar Dutra Zanotto**[2]

[1]Departamento de Física, Universidade Federal de São Carlos, São Carlos, Brazil

[2]Department of Materials Engineering, CERTEV — Center for Research, Technology, and Education in Vitreous Materials, Federal University of São Carlos, São Carlos, Brazil

Correspondence
Benjamin J. A. Moulton
Email: benmoul@df.ufscar.br

Funding information
São Paulo Research Foundation, Grant/Award Number: 2016/18567-5, 2016/15962-0, 2013/07793-6; Federal Agency for the Support and Improvement of Higher Education (CAPES), Grant/Award Number: PNPD20131474, 33001014004P9; CNPq

Abstract

The homogeneous and stoichiometric crystallization of the barium disilicate ($BaSi_2O_5$) glass makes it possible to follow the structural evolution of Raman bands from the supercooled liquid to the crystalline phase. We monitored the crystallization of supercooled liquid $BaSi_2O_5$ at 790°C over 440 minutes revealing a three-stage crystallization process: stage 1 involves changes in the barium sites toward a bonding environment that is similar to that in orthorhombic low barium disilicate. The end of stage 1 is marked by the loss of the Q^4 species vibration at 1170 cm^{-1} and the creation of a crystalline band at 490 cm^{-1}. Stage 2 is marked by the transition of the Q^3 peak (1060 cm^{-1}) from a Gaussian-like to a Lorentzian curve, indicating the formation of well-developed sheet structures. These observations lead us to conclude that the Raman spectra are resolving both the crystalline L-BS2 phase and the BS2 melt. The final stage involves a rapid decrease in the remaining Q^n species to form Q^3. This crystallization process involves structural modifications that occur on the tens of microns scale. The barium cations drive the initial stages of crystallization, providing direct evidence that the short-range order, around network modifiers, is a critical factor involved in homogeneous crystallization.

KEYWORDS
barium disilicate, crystal growth, crystallization, glass, Raman spectroscopy, silicate, structure, supercooled liquid

1 | INTRODUCTION

Understanding the crystallization process of glass-forming liquids is very relevant from both scientific and technological perspectives. While there is intense activity regarding crystal nucleation, growth, and overall crystallization kinetics, unfortunately, there have been scarce studies on the finest structural details of the crystallization pathways in supercooled liquids (SCL). The $BaO\text{-}2SiO_2$ (BS2) composition is one of a few stoichiometric glass-forming liquid that reveals homogeneous, internal crystal nucleation around the glass transition temperature (T_g)[1-6] and thus serves as a model for crystallization studies. Crystallization of the supercooled BS2 liquid is complex and it often crystallizes in an axiolitic or spherulitic morphology.[1,2,7,8] Ramsden and James[1,2] studied the early stages of the crystallization of a BS2 glass by transmission electron microscopy. During the initial stage of crystallization, these authors identified small spheres (<10 nm) composed of fine fibrillar crystallites, which were identified as the monoclinic polymorph, H-BS2. From these small H-BS2 crystals, the spherulitic growth of the orthorhombic sanbornite (L-BS2) grow. The BS2 crystal structure data shows that the orthorhombic L-BS2 phase has only one site each for Ba and Si, whereas monoclinic H-BS2

Prof. ED Zanotto's ACerS membership no. is 1092305.

 © 2018 The American Ceramic Society and Wiley Periodicals, Inc

has two Ba sites and three Si sites.[9] Both of these minerals are sheet silicates where the tetrahedra are linked by three corners (Q^3) or bridging oxygens (BO), parallel to their [001] plane. In addition to H-BS2, other studies on BS2 have provided evidence for the formation of small amounts of $Ba_5Si_8O_{21}$ and $Ba_3Si_5O_{13}$ phases during crystallization of the stoichiometric BS2.[10-12] The role of these metastable phases in the crystal nucleation and growth processes is still poorly understood and warrants further investigation beyond this study.[2,7]

The sensitivity of Raman spectroscopy to monitor the BS2 crystallization process was shown by Rodrigues et al.,[13] however, the structural evolution of supercooled liquid and the crystallization process itself were not investigated. Raman spectroscopy is among the most sensitive techniques to the local and medium-range order within silicate glasses and melts.[14-16] The majority of the vibrational modes for silicates are well known, although there remain some discrepancies in the detailed peak assignments.[16] Nonetheless, there is broad agreement that there are four main regions within the Raman spectra of silicate melts (e.g.[14,16]). At low wave numbers, below ~250 cm^{-1} the Boson peak is observed in all amorphous silicate materials.[17] Although its origin is still debated, it is a signature of the amorphous state whether as a glass or SCL.[13,17,18] In silica-poor alkaline earth-bearing silicates, the region from 200 to 400 cm^{-1} is dominated by oxygen vibrations associated with the modifier polyhedra, whereas in silica-rich compositions there are additional vibrations related to the bridging oxygen rocking and stretching vibrations.[14,16] At intermediate frequency shifts, between 400 and 800 cm^{-1}, lies the region assigned to symmetric stretching of the bridging oxygens (BO).[14,19]

The high-frequency region is dominated by symmetric stretching vibrations assigned to the non-bridging oxygen vibrations (NBO) located on the Q^n species; where "n" is the number of BO per silicon tetrahedron.[14,16,19] The Q^{0-3} band centers are separated by 50-100 cm^{-1} and show a remarkable consistency over a broad compositional range.[14,20] At room temperature, the Q^{1-3} band centers are well established around 900, 975, and 1075 cm^{-1} ($\pm$25 cm^{-1}), respectively.[14,20] In the BS2 spectrum at 790°C, the Q^n bands show a negative shift of 10-18 cm^{-1} from their respective room temperature positions. Therefore, at 790°C, the major bands at 920 and 1060 cm^{-1} are assigned to the Q^2 and Q^3 bands. Despite the clear consistency in band position, additional bands are required to fit the complete spectral envelope (e.g.[21,22]). Two possible explanations have been provided for these additional bands. The first possibility is that the each Q^n band has two (or more) associated vibrations and the relative position of these bands is determined by the connectivity of the adjacent tetrahedral network (c.f.[21]). For example, a Q^3 species attached to other Q^3 species has a higher frequency shift than a Q^3 attached to Q^2 species. The second possibility is that additional bands arise from the presence of modifier cations (c.f.[22,23]). Where present, modifiers will weaken the Si-BO bond causing a decrease in the associated force constants via charge transfer from the modifier onto the central Si atom.[23] Both explanations appear plausible and are not necessarily mutually exclusive. The implications for the spectral evolution of BS2 are discussed below.

In this article, we present a detailed, time-resolved in situ analysis of the crystallization of BS2 using Raman scattering. One crucial observation is that BS2 crystallizes homogeneously and arguably stoichiometrically. Therefore, unlike non-stoichiometrically crystallizing systems, the Raman vibrational modes evolve directly from those in the supercooled liquid to those in the crystal. As a result, a novel behavior is resolved. Three distinct stages in the transformation of the SCL to the crystalline orthorhombic L-BS2 exist, and their structural characteristics are reported.

2 | METHODS

The BS2 glass composition used in this research was synthesized by splat cooling from the melt. The full preparation has been described in Rodrigues et al.[8,13] The composition of our glass has been measured by electron probe microanalyzer (EPMA) on a JEOL JXA8230 5-WDS using a 15 nA current and 15 kV voltage on a 1 μm spot size. Our BS2 glass has the composition $33.8BaO{\cdot}66.2SiO_2$. See Table S1 for the full chemistry. Cubic specimens of uniform thickness (2.0 × 2.0 × 1.5 mm), devoid of bubbles were chosen for this high-temperature experiment. Using a heating rate of 10 K/min, differential scanning calorimetry (DSC) results show that the glass transition temperature (T_g) and the two crystallization peaks of this glass which reveal them to be 690°C, 853°C, and 905°C, respectively.[8] One sample was heated at a rate of 25°C/min from 25°C up to 790°C ($\pm$5°C) and held constant for 440 minutes during the experiment. At this temperature for BS2 glass, the crystallized fraction is mostly a consequence of the growth of pre-existing crystals (which formed during the quenching and heating procedures) in the volume.[24] By applying the Avrami equation to existing experimental nucleation and growth rate data[8,24,25] we calculate that after 440 minutes at 790°C the volume fraction crystallized is 99%. Moreover, the surface layer of crystals is only 3 μm in thickness after 440 minutes. We refer the reader to Figure 1B of reference[8] to view an example of surface and internal crystallization in BS2 glass. In this study, the sample overwhelmingly crystallizes from within the SCL volume rather than the surface. It truly exhibits internal crystallization.

In situ Raman spectra were taken with a HORIBA LabRAM HR800 Evolution mounted with a Linkam HS1500 micro-furnace. The 532 nm line of a diode laser was used.

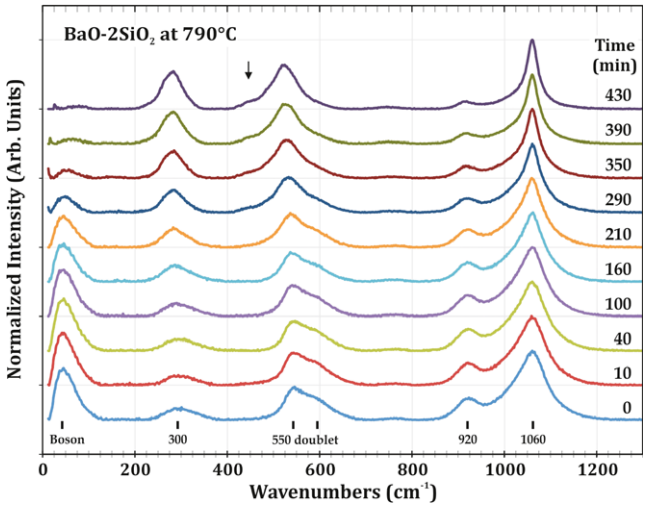

FIGURE 1 Characteristic Raman spectra vs time at 790°C. Spectra have been background corrected, and intensity normalized to the 1060 cm^{-1} peak. The arrow at 490 cm^{-1} indicates the position of a new peak which appears near 210 min and is clearly a shoulder after 300 min (see discussion below) [Color figure can be viewed at wileyonlinelibrary.com]

The same results were obtained using the 633 nm laser. To approximate the sampling volume the depth of field (d.o.f. = 4 λ/N.A.^{2}) and the spot size (D = 1.22 λ/N.A.) were calculated to be 15.9 and 1.70 μm, respectively.[26] With a probe depth of roughly 16 μm, we can be sure that the Raman signal is dominantly coming from within the volume of the SCL and therefore, faithfully records the internal crystallization rather than surface crystallization. The furnace temperature was stable and never varied more than 1°C during the 435 minutes. A spectrum was taken over 5 minutes (five accumulations of one minute each) approximately every 10 minutes. Data points are plotted at the middle point of the acquisition time. For example, the spectra from 210 minutes to 215 minutes are plotted at the 212.5 minutes mark. The spectra were curve fit to quantify the peak behaviors during crystallization. To curve fit the data in a consistent manner a background was removed using a polynomial spline fit between the four peak regions. This process results in a flat background with Raman peaks in the regions <100 cm^{-1}, 200-400 cm^{-1}, 425-700 cm^{-1}, and 850-1300 cm^{-1} in the BS2 supercooled liquid. Each spectrum was then intensity normalized to the most intense peak, found at ~1060 cm^{-1}.

Curve fitting of the spectra enables us to quantify changes in the peak behaviors. Peak areas were normalized relative to the maximum area of their respective region. The spectra were fit using a Lognormal line shape for the Boson peak and Gaussian line shapes for the rest of the peaks except the 1060 cm^{-1} peak. The 1060 cm^{-1} peak, is the most intense peak within crystalline sanbornite (L-BS2) and has a Lorentzian line shape, typical of crystalline materials (c.f.[27]). In contrast, silicate glasses and melts are best fit by Gaussian line shapes, although the line shape may be up to 30% Lorentzian without significantly affecting the quality of the fit.[27] In the case of BS2 and crystalline sanbornite (L-BS2), both have the same Raman peak position at 1060 cm^{-1}, but the line shape was permitted to vary between Gaussian and Lorentzian using a pseudo-Voigt curve. The pseudo-Voigt lineshape contains a parameter that varies from 0 for a Gaussian curve to 1 for a Lorentzian curve. To fit the remaining Q^n species bands, we constrained the full-width at half-the-maximum-intensity (FWHM) to be roughly equal, between 45 and 65 cm^{-1}. This range is consistent with recent high-temperature work on alkali-bearing silicate SCL.[22] The FWHM of the intense 920 and 1060 cm^{-1} peaks were permitted to vary to assess the validity of this constraint. The resulting FWHMs remain within the 45-65 cm^{-1} limits. A consequence of this is that the high-frequency side of the 1060 cm^{-1} peak required two additional curves centered at 1120 and 1172 cm^{-1}. The latter peak at 1172 cm^{-1} is very weak and constitutes only 1% the area of this region. To go from the Raman band areas to the Q^n species fraction a correction factor has been applied; for more details see Appendix S1.

A two-step curve fitting procedure was used on the 425-700 cm^{-1} region, which includes the 550 doublet (see below). The 550 doublet was first to fit without constraints and then re-fit based on the results of the initial free-fit using the main peak center as the only constraint (Appendix S2). For all curve fits, the Levenberg-Marquardt regression was done using Fityk software.[28]

3 | RESULTS AND DISCUSSION

BS2 glass and supercooled liquid Raman spectra (SCL) have been previously reported in several studies.[11,13,29,30] Our spectra are qualitatively the same as previous studies and are compared to L-BS2 reference spectra (Figure 2). It is clear that the Boson peak intensity decreases throughout the crystallization process (Figure 3). The peak centered at 300 cm^{-1} (Figure 4) and the doublet found at 550 cm^{-1} (Figure 5) both display a slight shift to lower frequencies and an increase in their intensities during crystallization. In contrast, the peaks at 920 and 1060 cm^{-1} remain at apparently constant positions while their intensities decrease and increase, respectively (Figures 6 and 7). The latter behavior is expected as the crystalline L-BS2 has a single sharp peak near 1060 cm^{-1} (Figure 2).[13]

The Boson peak center shows a non-linear behavior, shifting dramatically to higher wavenumbers after the first 200 minutes. Its area displays a more distinct behavior. The area of the Boson peak appears to continuously decrease from 60 minutes until the 350 minute mark. The Boson peak area decreases at a rate of 0.25% per minute and then decreases to

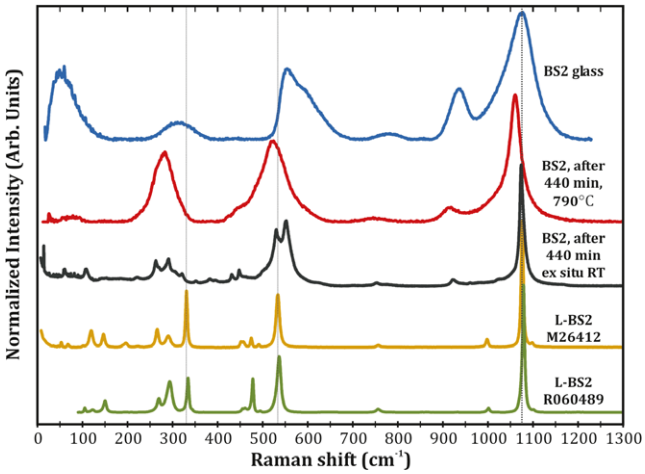

FIGURE 2 Raman spectrum of BS2 glass, L-BS2 (sanbornite) and the Raman spectrum at 440 min from Figure 1 and its ex situ spectrum outside of the furnace at room temperature (RT) (may not be identical position to that of the in situ spectrum). The L-BS2 spectrum R060489 comes from the RRUFF database[31] whereas the L-BS2 spectrum, M26412, is a sanbornite sample from the Royal Ontario Museum [Color figure can be viewed at wileyonlinelibrary.com]

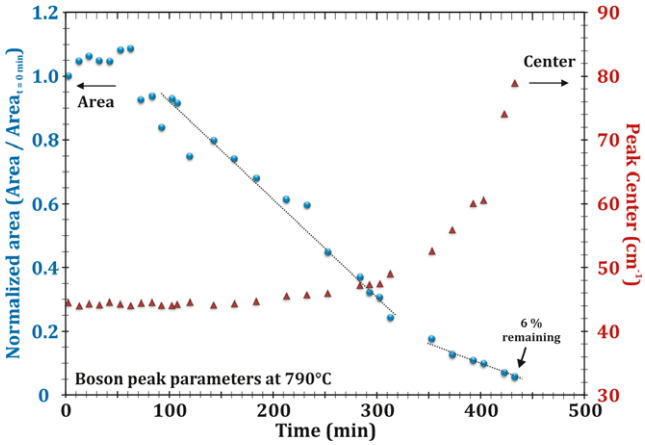

FIGURE 3 Boson peak (<100 cm^{-1}) parameters vs time. The peak area (circles) and center (triangle) of the log-normal peak are reported. Each area has been normalized to the peak area at t = 0 min. Dashed lines are just to guide the eye [Color figure can be viewed at wileyonlinelibrary.com]

~0.1% per minute after 350 minutes. Although its origin remains controversial, the Boson peak reveals the overall degree of disorder which suggests that even after the 435 minutes in this experiment there remains some BS2 in the SCL state.[18,32-34] Therefore, the Boson peak shows no evidence of crystallization during the first 60 minutes of this experiment. This 60 minutes delay is observed in the behavior of all other Raman peaks and suggests that no structural changes are revealed within the Raman spectra during this time. An induction time of 35 minutes is expected for crystallization at 790°C based on the experimentally available data.[8]

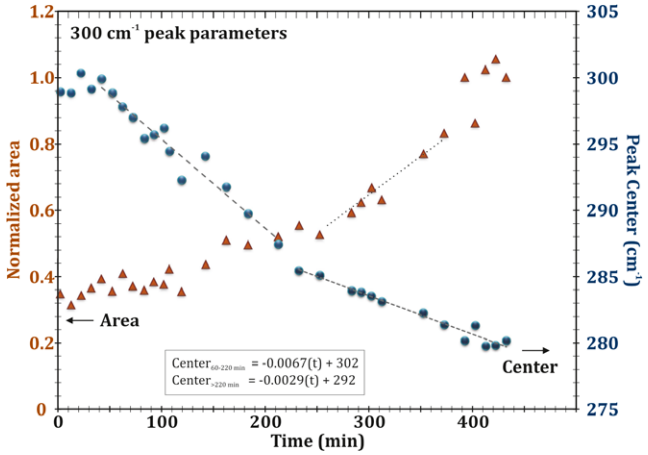

FIGURE 4 300 cm^{-1} peak parameters during crystallization. The peak area is normalized relative to the final peak area (t = 435 min). The error associated with reproducibility of the curve fit is smaller than the symbols [Color figure can be viewed at wile yonlinelibrary.com]

3.1 | Crystallization Stage 1 (60-210 minutes): Structural reorganization of the SCL

After the initial 60 minutes, crystallization starts, the Boson peak area diminishes, and the vibrations associated with barium polyhedral and NBOs display distinct changes in behavior. The slight increase in the 300 cm^{-1} peak area and the acute decrease in its peak center (Figure 4) suggest there is a significant difference between the local environment of the Ba ions in the SCL compared to those in the L-BS2 phase. The 1060 cm^{-1} peak starts to become slightly more Lorentzian, and its FWHM starts to decrease linearly (Figure 7). While the 1060 cm^{-1} peak (Q^3) becomes sharper, it is not accompanied by an increase in area (Figure 8). In fact, the Q^3 band shows a modest decrease of ~5% to the benefit of Q^4 species (Figure 8). There appears to be no effect on the Q^2 species indicating a modest polymerization of the silicate network during this stage. This idea may be counter-intuitive since polymerization is expected to decrease the mobility of elements, thereby impeding crystallization, but can be explained by the polymerization reaction proposed by Nesbitt and co-workers: $Ba\text{-}2Q^3 \leftrightarrow 2Q^4 + Ba^{2+} + O^{2-}$.[18] In this case, the polymerization enhances diffusion of itinerant species, O^{2-} and Ba^{2+} ions, that are able to modify and reorganize the silicate network facilitating crystallization.

These observations suggest that itinerant Ba cations and polymerization of the Q^3 environments are important during the early stages. The strong negative shift in the peak center of the Ba vibrations at 300 cm^{-1} indicates that the bond strength, and therefore the force constants, decrease from the SCL relative to the crystalline vibrations. The fact that the Ba vibrations attain the near-crystalline frequency while there is only a negligible increase in the peak area suggests that, while they probably attain a crystal-like

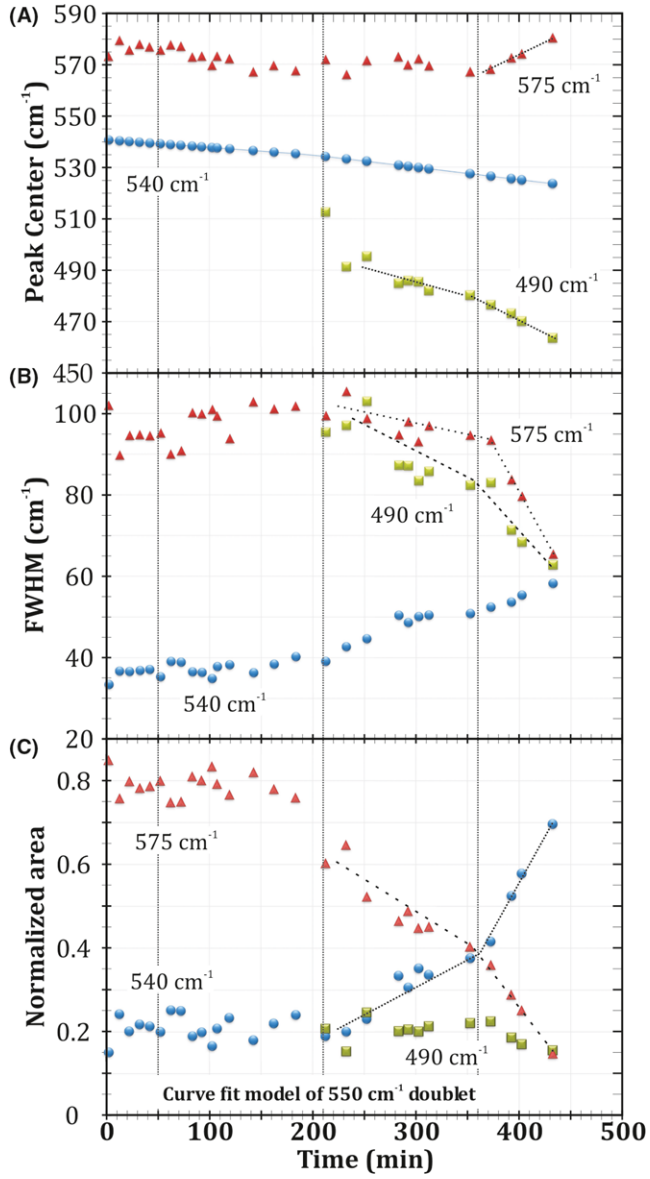

FIGURE 5 Revised curve fit using the 540 cm^{-1} band peak center constraint (Figure S1). A, The peak centers. B, The full-width at half-the-maximum intensity (FWHM). C, The normalized areas of the three peaks (squares - 490 cm^{-1}; circles - 540 cm^{-1}; triangles - 575 cm^{-1}). Note that the 540 cm^{-1} peak attains 70% of the peak intensity at the end [Color figure can be viewed at wileyonlinelibrary.com]

coordination (C.N. = 9), these sites remain quite distorted. Moreover, the lack of modification to the BO vibrations during this stage indicates that the modifier-rich regions within the SCL are driving the initial stage of crystallization. Finally, these modifications appear to be widespread throughout the network as they involve the complete shift in the band and not simply the addition of new vibrational modes. Therefore, this organization is not simply a local phenomenon around the crystal nuclei but a pervasive change throughout the silicate network.

3.2 | Crystallization Stage 2 (210-370 minutes): From Supercooled Liquid to Q^3 sheets

This stage reveals a major reorganization of the silicate network, which affects all Raman bands. The Ba-associated peak at 300 cm^{-1} shows a decrease in the rate of shift and an increase in area (Figure 4). In fact, the 300 cm^{-1} band essentially attains its final intensity which is roughly equal to that of the BO vibrations at 500 cm^{-1}. The intermediate frequency bands, which formed the 550 doublet, now require a third peak centered at 490 cm^{-1} to fit the spectral envelope while the areas and the FWHM of the original two bands change dramatically. The 540 cm^{-1} band shows an increase in both area and FWHM while the 575 cm^{-1} band displays a decrease in both parameters (Figure 5). The high-frequency region displays a loss of the weak band at 1170 cm^{-1} while the 1060 cm^{-1} band becomes completely Lorentzian and increases in intensity (Figure 6, 7 and 8). The Q^2 and Q^4 bands experience a weak decrease in their respective proportion (Figure 8). Finally, we note that the Q^n species presented in Figure 8 does not accurately represent the proportion of Q^n species because of the 1060 cm^{-1} band, the Q^3 band, includes both the signal from Q^3 species within the SCL as well as that of the crystal. These observations indicate that the Raman spectra simultaneously record both the crystal formation and retain the amorphous signatures of the Q^n bands and Boson peak.

The relative intensities of the 300, 550, and 1060 cm^{-1} peaks suggest a structure which has equal contributions from BaO_x polyhedra and BO vibrations with well-developed sheets of Q^3 species. We interpret this as the growth of L-BS2 as its crystal structure has only a single site for each Ba and Si. The decreasing FWHM and increasing area of the 1060 cm^{-1} peak indicates the presence of well defined Q^3 sites, but the remaining Q^n species indicate that some tetrahedral sheets may be cross-linked by $Q^{2\text{-}4}$ species. Alternatively, the $Q^{2\text{-}4}$ signature could solely be from the SCL signal. The persistence of all Q^n bands in the roughly same proportion suggests that there is no preference for which species are incorporated into the crystal or that the bulk melt connectivity does not change on the larger scale.

The presence of well-formed sheets of Q^3 species implies that the BO environments should also be well defined (Figure 5). Indeed, the 550 doublet displays indications of a more crystalline-like environment. For instance, the area and the FWHM of the 540 cm^{-1} peak increase during this period whereas the 575 cm^{-1} band, that was originally the strongest signal within this doublet, decreases steadily (Figure 5). Moreover, during the crystallization process, we observe the FWHM of the BO vibrations converge to 60 cm^{-1} around 430 minutes (Figure 5). This behavior indicates that the BO environments between SCL and crystal are quite different. The weak changes in the peak centers suggest that the bond strength does not change dramatically, but the other

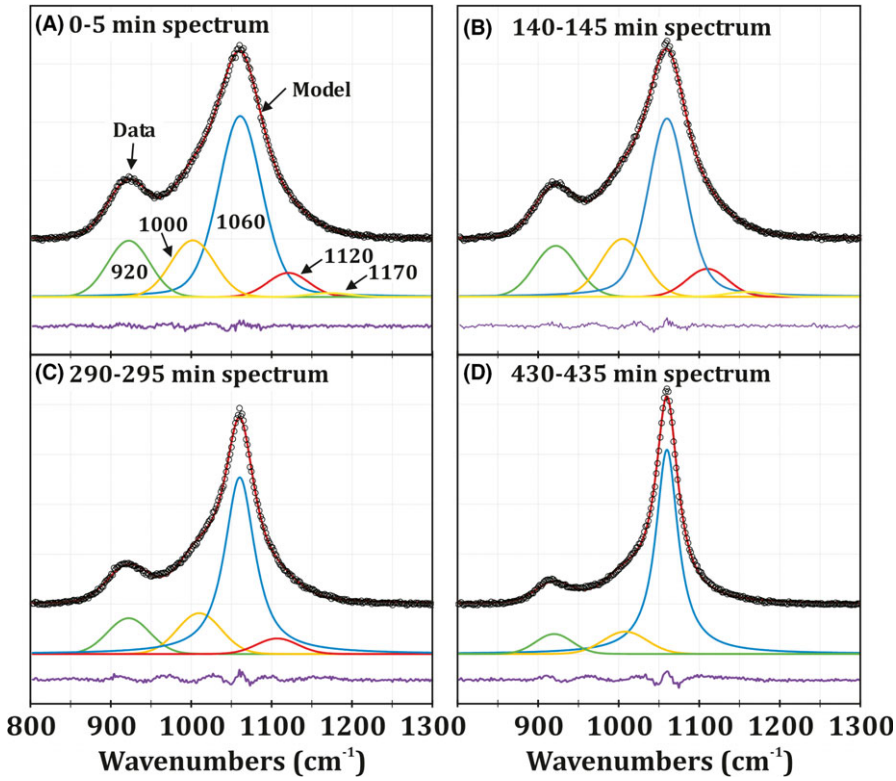

FIGURE 6 Example curve fits of Raman spectra taken during crystallization at t = 0 min (A), t = 140 min (B), t = 290 min (C), t = 430 min (D). For colors see the digital version. The fit curves are the 920, 1000, 1060, 1120, and 1170 cm^{-1} from left to right in each example and are labeled in (A). Note the loss of higher frequency peaks in (C) and (D) [Color figure can be viewed at wileyonlinelibrary.com]

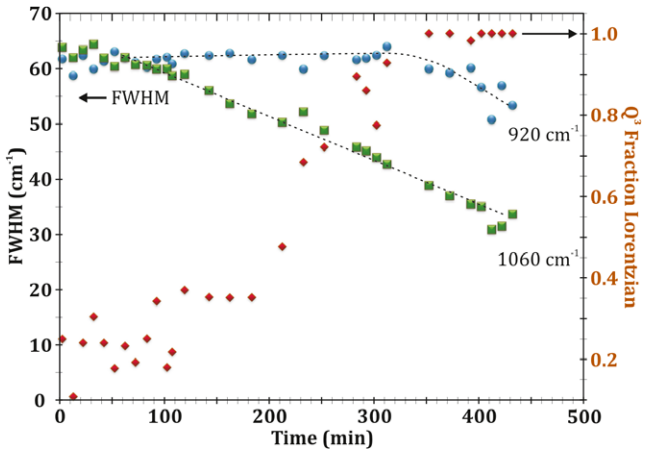

FIGURE 7 FWHM of the 920 (blue circles) and 1060 cm^{-1} (green squares) bands and the Lorentzian character (red diamonds) of the 1060 cm^{-1} band. Note that the 1060 cm^{-1} band reaches a completely Lorentzian character well before crystallization is finished. The maximum FWHM of the 920 cm^{-1} band does not appear to change until the 1060 cm^{-1} band becomes completely Lorentzian [Color figure can be viewed at wileyonlinelibrary.com]

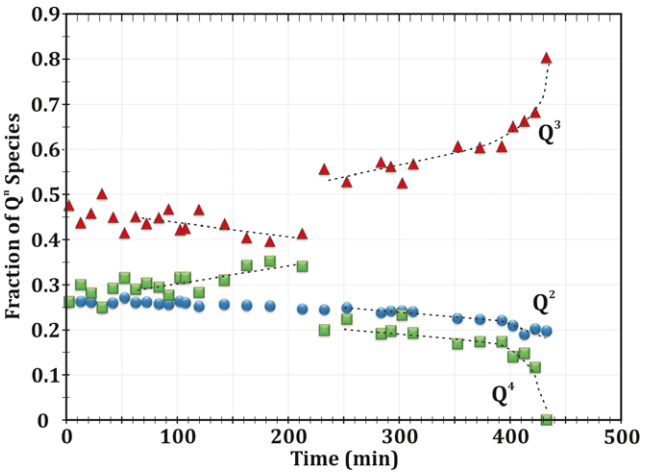

FIGURE 8 Fractions of Q^2 (circle), Q^3 (triangles), and Q^4 (square) species. See Appendix S1 for details of the Q^n calculation. Dashed lines are guides to the eye. The errors associated with the reproducibility of the curve fit are much smaller than the symbols [Color figure can be viewed at wileyonlinelibrary.com]

parameters indicate that the proportions of the BO environments decrease as expected during the crystallization process.

One distinct change at 210 minutes, is that the high-frequency region no longer requires the highest-frequency shifted Q^4 band, at 1170 cm^{-1}, while at the same point in time, the 550 doublet region requires an additional band at 490 cm^{-1} to adequately fit the spectral envelope. The 490 cm^{-1} band, which constitutes 20% of the intensity, appears to reduce the intensity of the 575 cm^{-1} band by a similar magnitude. After the appearance of the 490 cm^{-1}

band at the 210 minute mark, the 575 cm^{-1} band proceeds to decrease in area in proportion to the increase in the area of the 540 cm^{-1} band. The latter behavior can be interpreted as the formation of BO environments within the L-BS2 structure at the expense of the environments within the SCL. The 490 cm^{-1} band is tentatively assigned to the vibrations in L-BS2 which are found in this region (Figure 2). Vibrational modes in this region are typically assigned to internal deformation modes associated with the Si_2O_5 sheet(s) [c.f.[35,36]] and indicate that the Raman spectrum is recording a crystalline signal from this point onwards. This interpretation is consistent with the observations that the lineshape of the 1060 cm^{-1} band (Figure 7) and the proportion of Q^3 species increases at this point (Figure 8).

3.3 | Crystallization Stage 3 (370-435 minutes): Complete crystallization

While we note the Boson peak still has 6% of its initial area, we speculate that the processes observed in the remaining hour of our experiment will continue until completion; producing a completely crystalline sample. Indeed, the post-run sample measured at room temperature shows no evidence for the Boson peak, although the Raman bands are quite broad indicating that the crystals are small (Figure 2). In the final stage, the 300 cm^{-1} peak shifts to slightly lower frequencies, from 285 to 280 cm^{-1} (Figure 4) while the high-frequency bands begin to noticeably decrease to the benefit of the 1060 cm^{-1} band (Q^3 - Figure 7 and 8). During this stage, it appears that the non-Q^3 bands convert to crystalline Q^3 species, while the other weaker bands in the 550 doublet convert to the 540 cm^{-1} vibrations (Figure 5). All of these observations point to the rapid conversion of the remaining SCL to crystalline L-BS2 (orthorhombic sanbornite).

4 | CONCLUSIONS

The crystallization pathway of supercooled barium disilicate liquid displays a three-stage process: In the first stage, the local environment around the network modifier polyhedra shows a clear structural reorganization, likely involving itinerant Ba^{2+}, and polymerization of the silicate network, while at the end of this stage some Q^4 species disappear. The second stage is dominated by a modification of the bridging oxygen environment and associated development of sheets of Q^3, as found in the orthorhombic L-BS2. The final stage sees the rapid consumption of the remaining supercooled liquid network to form the crystalline phase. Our results provide no clarity on the role of non-stoichiometric phases (e.g. $Ba_3Si_5O_{13}$) in the crystallization process and we are currently pursuing experiments to clarify this debate. Our results show that the crystallization pathway of barium disilicate involves a series of structural rearrangements, which are pervasive throughout the entire silicate network, on the tens of microns scale. The observation that barium ions drive the initial stage of crystallization provides direct evidence that the short-range order around the network modifier is one of the critical factors involved in homogeneous crystallization.[37] This study of the finest structural details of the crystallization pathway in a glass-forming oxide contributes to a better understanding of this important phenomenon. It would be insightful to carry out a similar study with other oxide compositions that undergo internal homogeneous nucleation, such as $Li_2O{\cdot}SiO_2$, $CaO{\cdot}SiO_2$, and $Li_2O{\cdot}2B_2O_3$ to generalize (or not) these findings.

ACKNOWLEDGMENTS

BJAM and DVS thank the São Paulo Research Foundation (FAPESP) for funding this research under the grant no. 2016/18567-5 and 2016/15962-0. AMR thank the Federal Agency for the Support and Improvement of Higher Education (CAPES), grant number PNPD20131474 - 33001014004P9. We appreciate the support of CNPq and CAPES support to PSP. Finally, we thank FAPESP for the CEPID project funding (no. 2013/07793-6). We kindly thank Dr. Kim Tait and Veronica Di Cecco for the sanbornite sample from the Royal Ontario Museum (ROM), Toronto, ON, Canada. We thank two anonymous reviewers for their constructive comments.

ORCID

Benjamin J. A. Moulton http://orcid.org/0000-0003-3332-7977
Alisson Mendes Rodrigues http://orcid.org/0000-0003-0449-9219
Paulo Sergio Pizani http://orcid.org/0000-0002-5914-1671
David Vieira Sampaio http://orcid.org/0000-0002-6144-4794
Edgar Dutra Zanotto http://orcid.org/0000-0003-4931-4505

REFERENCES

1. Ramsden AH, James PF. The effects of amorphous phase separation on crystal nucleation kinetics in BaO-SiO_2 glasses - Part 1 general survey. J Mater Sci. 1984;19:1406–1419.
2. Ramsden AH, James PF. The effects of amorphous phase separation on crystal nucleation kinetics in BaO-SiO2 glasses - Part 2 isothermal heat treatments at 700 C. J Mater Sci. 1984;19:2894–2908.
3. Zanotto ED, James PF. Experimental test of the general theory of transformation kinetics: homogeneous nucleation in a BaO·2SiO2 glass. J Non Cryst Solids. 1988;104:70–72.
4. Abyzov AS, Fokin VM, Rodrigues AM, Zanotto ED, Schmelzer JWP. The effect of elastic stresses on the thermodynamic barrier for crystal nucleation. J Non Cryst Solids. 2015;432:325–333.

5. Fokin VM, Abyzov AS, Zanotto ED, Cassar DR, Rodrigues AM, Schmelzer JWP. Crystal nucleation in glass-forming liquids: variation of the size of the 'structural units' with temperature. J Non Cryst Solids. 2016;447:35–44.
6. Abyzov AS, Fokin VM, Yuritsyn NS, Rodrigues AM, Schmelzer JWP. The effect of heterogeneous structure of glass-forming liquids on crystal nucleation. J Non Cryst Solids. 2017;462:32–40.
7. Lewis MH, Smith G. Spherulitic growth and recrystallization in barium silicate glasses. J Mater Sci. 1976;11:2015–2026.
8. Rodrigues AM, Cassar DR, Fokin VM, Zanotto ED. Crystal growth and viscous flow in barium disilicate glass. J Non Cryst Solids. 2018;479:55–56.
9. Hesse KF, Liebau F. Crystal chemistry of silica-rich barium silicates, III: refinement of the crystal structures of the layer silicates $Ba_2[Si_4O_{10}]$ (I), (Sanbornite), and $Ba_2[Si_4O_{10}]$ (h). Zeitschrift für Krist - Cryst Mater. 1980;153:33–41.
10. Takahashi Y, Osada M, Masai H, Fujiwara T. Transmission electron microscopy and in situ raman studies of glassy sanbornite: an insight into nucleation trend and its relation to structural variation. J Appl Phys. 2010;108:063507.
11. Takahashi Y, Ihara R, Fujiwara T, Osada M. Crystallization and morphology of glassy sanbornite. Key Eng Mater. 2011;485:301–304.
12. Herrmann A, Simon A, Rüssel C. Preparation and luminescence properties of Eu^{2+}-doped $BaSi_2O_5$ glass-ceramics. J Lumin. 2012;132:215–219.
13. Rodrigues AM, Rino JP, Pizani PS, Zanotto ED. Structural and dynamic properties of vitreous and crystalline barium disilicate: molecular dynamics simulation and raman scattering experiments. J Phys D Appl Phys. 2016;49:435301.
14. McMillan PF. Structural studies of silicate glasses and melts-applications and limitations of raman spectroscopy. Am Mineral. 1984;69:622–644.
15. Rossano S, Mysen B. Raman spectroscopy of silicate glasses and melts in geological systems. Raman Spectrosc Appl Earth Sci Cult Herit 2012;12:321–366.
16. Neuville DR, de Ligny D, Henderson GS. Advances in raman spectroscopy applied to earth and material sciences. Rev Mineral Geochemistry. 2014;78:509–541.
17. McMillan PF, Wolf GH, Poe BT. Vibrational spectroscopy of silicate liquids and glasses. Chem Geol. 1992;96:351–366.
18. Gurevich VL, Parshin DA, Schober HR. Anharmonicity, vibrational instability, and the Boson peak in glasses. Phys Rev B. 2003;67:94203.
19. Matson DW, Sharma SK, Philpotts JA. The structure of high-silica alkali-silicate glasses. A raman spectroscopic investigation. J Non Cryst Solids. 1983;58:323–352.
20. Nesbitt HW, Bancroft GM, Henderson GS, Richet P, O'Shaughghnessy C. Melting, crystallization, and the glass transition: toward a unified description for silicate phase transitions. Am Mineral. 2017;102:412–420.
21. Koroleva ON, Anfilogov VN, Shatskiy A, Litasov KD. Structure of Na_2O-SiO_2 melt as a function of composition: in situ Raman spectroscopic study. J Non Cryst Solids. 2013;375:62–68.
22. O'Shaughnessy C, Henderson GS, Nesbitt HW, Bancroft GM, Neuville DR. Structure-property relations of caesium silicate glasses from room temperature to 1400 K: implications from density and Raman spectroscopy. Chem Geol. 2017;461:82–95.
23. Nesbitt HW, Henderson GS, Bancroft GM. Electron densities over Si and O atoms of tetrahedra and their impact on Raman stretching frequencies and Si-NBO force constants. Chem Geol. 2017;461:65–74.
24. Rodrigues AM. Diffusion processes, crystallization and viscous flow in barium disilicate glass. Ph.D thesis, São Carlos: Federal University of São Carlos; 2014.
25. Zanotto ED, Galhardi A. Experimental test of the general theory of transformation kinetics: homogeneous nucleation in a $Na_2O{\cdot}2CaO{\cdot}3SiO_2$ glass. J Non Cryst Solids. 1988;104:73–80.
26. Neuville DR, Cormier L, Caurant D, Montagne L. *From glass to crystal nucleation, growth and phase separation: from research to applications*. Les Ulis Cedex, France: EDP Sciences; 2017.
27. Tribaudino M, Montovani L, Bersani D, Lottici P. Raman spectroscopy of (Ca, Mg) $MgSi_2O_6$ clinopyroxenes. Am Mineral. 2012;97:1339–1347.
28. Wojdyr M. Fityk: a general-purpose peak fitting program. J Appl Crystallogr. 2010;43:1126–1128.
29. Mysen BO, Frantz JD. Structure of silicate melts at high temperature: in-situ measurements in the system BaO-SiO_2 to 1669 C. Am Mineral. 1993;78:699–709.
30. Frantza J. Raman spectra and structure of BaO-SiO2 SrO-SiO2 and CaO-SiO2 melts to 1600 C. Chem Geol. 1995;121:155–176.
31. Lafuente B, Downs RT, Yang H, Stone N. The power of databases: the RRUFF project. In: Armbruster T, Danisi RM, editors. Book chapter in *Highlights in Mineralogical Crystallography*. Berlin, München, Germany: DE Gruyter; 2016: pp. 1–30.
32. Elliott SR. A unified model for the low-energy vibrational behaviour of amorphous solids. Europhys Lett. 2007;19:660–660.
33. Duval E, Mermet A, Leparc R, Champagnon B. About the origin of the boson peak in vitreous silica. Philos Mag. 2004;84:1433–1436.
34. Champagnon B, Wondraczek L, Deschamps T. Boson peak, structural inhomogeneity, light scattering and transparency of silicate glasses. J Non Cryst Solids. 2009;355:712–714.
35. Brawer SA, White WB. Raman spectroscopic investigation of the structure of silicate glasses. I. The binary akali silicates. J Chem Phys. 1975;63:2421–2432.
36. Richet P, Mysen BO, Ingrin J. High-temperature X-ray diffraction and raman spectroscopy of diopside and pseudowollastonite. Phys Chem Miner. 1998;25:401–414.
37. Zanotto ED, Tsuchida JE, Schneider JF, Eckert H. Thirty-year quest for structure–nucleation relationships in oxide glasses. Int Mater Rev. 2015;60:376–391.

SUPPORTING INFORMATION

Additional supporting information may be found online in the Supporting Information section at the end of the article.

How to cite this article: Moulton BJA, Rodrigues AM, Pizani PS, Sampaio DV, Zanotto ED. A Raman investigation of the structural evolution of supercooled liquid barium disilicate during crystallization. *Int J Appl Glass Sci*. 2018;9:510–517. https://doi.org/10.1111/ijag.12356